Analysis of the Hybrid PSO-InC MPPT for Different Partial Shading Conditions

André Luiz Marques LEOPOLDINO[1], Cleiton Magalhães FREITAS[2], Luís Fernando Corrêa MONTEIRO[1]
[1]*Post-graduate Program of Electronic Engineering (PEL), Rio de Janeiro State University, Brazil*
[2]*Electrical Engineering Department, Rio de Janeiro State University, Brazil*
leopoldino@ieee.org, cleiton.freitas@uerj.br, lmonteiro@uerj.br

***Abstract*—This article addresses the Particle Swarm Optimization with Incremental Conductance algorithm (PSO-InC) performance as the maximum power point tracking algorithm (MPPT), when the photovoltaic system is under different partial shading patterns. The PSO-InC MPPT combines the global-searching capabilities of particle swarm optimization with the smoother search feature of the incremental conductance algorithm. The analysis proceeds from a systematic approach involving the system simulation for different Environmental conditions. Besides that, to accurately represent the effects of the inherent stochasticity of the PSO, diverse starting conditions were considered in each case. The main contribution, in this sense, consists of highlighting some PSC patterns that might compromise the effectiveness of the PSO, even though the average efficacy on searching the global MPP (GMPP) is over 89%. For instance, based on one of the exploited PSC patterns, one may note a decrement of the PSO effectiveness to a level as lower as 36%. This article also presents simulation results highlighting the PSO-InC MPPT dynamics under transient and steady-state conditions.**

***Index Terms*—hybrid intelligent systems, maximum power point trackers, particle swarm optimization, photovoltaic systems, solar power generation.**

I. INTRODUCTION

In the past few years, several worldwide governmental-backed policies fomented the photovoltaic generation, in general to overcome the Environmental effects caused by fossil fuels and other non-renewable energy resources. In this context, the global installed capacity of photovoltaic (PV) generation soared from under 75 GW to 312 GW between the years 2011 and 2017, according to [1-2], and the number is still ramping up. These changes paved the way for several researches addressing this topic, mostly focusing on the development of MPPT algorithms [3] and the integration of solar arrays to the power grids [4-5]. In this regard, a subfield that is yet in ongoing development is the crafting of control algorithms to search for the Maximum Power Point (MPP) when the PV panels are under Partial Shading Condition (PSC).

The PSC occurs when the PV panels present different radiance levels due to unregular shading patterns caused by Environmental conditions. In short, the PSC leads to the resulting Power x Voltage curve with multiple local MPPs [6-8]. It is important to comment that the number of MPPs is equal to or lower than the number of PV arrays. For example, a photovoltaic system based on 3 PV arrays may present a Power x Voltage curve with no more than three local MPPs. In this context, the MPPT algorithm must be capable to correctly finding the Global MPP (GMPP), without being trapped in local maxima. These algorithms are based on either the combination of regular MPPTs with crafted rules, such as in [9], or PSO [10-12] or following several other high-end approaches, as presented in [13].

In literature, there are several works involving PSO issues as global MPP. For instance [14-15] discuss the hyperparameters effects on the GMPP tracking. In these articles, the PSO was enabled whenever an increment or decrement of the produced power was greater than a pre-defined threshold. It is important to notice that enabling and disabling the PSO algorithm is a necessary action. Otherwise, a scattered pattern may appear in the produced power even when the algorithm converges. Unfortunately, this enabling/disabling approach leads to an efficiency loss, since the system starts a new time-consuming, PSO-based tracking even in uniform shading condition. In this context there are proposals involving different approaches of combining the PSO algorithm with other MPPT approaches, the so-called hybrid PSO-MPPTs. Sundareswaran et al. [16] presented a hybrid MPPT in which the PSO is combined with the perturb and observe (P&O) algorithm. In this case, the search for the GMPP is started with the PSO algorithm and as soon as its particles are within a narrow neighborhood around the best solution, the MPPT swaps over to the P&O. The inverse idea was considered by Lian et al [17], where they started using the P&O for reducing the searching domain of the PSO-MPPT. One example of hybrid MPPT encompassing PSO and an InC algorithm is the one introduced by Mirbagheri et al. [18]. In this paper, the authors proposed a strategy where the InC locates the MPP neighborhood, whereas the PSO is activated for refining the result. Unfortunately, this approach is not suitable for PV systems under PSC, in which case, the MPPT could be trapped in a local maximum. This approach of starting the PSO after an InC round is also presented by Abdulkadir and Yatin [19], though the authors used the InC to find one local MPP and reduce the searching range of the PSO algorithm, similarly with the idea presented in [17]. Differently from [18-19] presents no issues whatsoever with PSC and, in addition, provides a faster convergence. Nonetheless, the performance boost in [19] may only be applied to arrays with a small number of PV panels. Likewise [16], Manickam et al. [20] also proposed a hybrid MPPT combining the PSO and P&O, though their approach presents a series of rules to increases the speed of the GMPP tracking under PSC. Despite the distinguishing improvements in comparison to the traditional PSO algorithm, as far as we could understand, the setting of the rules may be cumbersome as the number of PV panels in an

Digital Object Identifier 10.4316/AECE.2022.02004

array grows. Jiying Shi et al. [21] proposed a hybrid MPPT algorithm in which a variant of the PSO-MPPT is used initially to perform a broader search, and afterward, the InC replaces the PSO to conduct a narrower search. Their major contribution is that during the PSO loop, some of the particles are put in dormant mode whenever they start searching the same neighborhood. This strategy provides a faster convergence in comparison to conventional PSO MPPTs.

Those articles provided results that highlighted the effectiveness of hybrid PSO-MPPT algorithms, though their analysis follows a more microscopic approach. In this paper, on the other hand, we gathered results involving the PSO-MPPT performance related to different shading patterns. The major contribution, in this sense, was to evaluate that some PSC patterns might compromise the PSO effectiveness, even though the average efficacy on searching the GMPP is over 89%. In this context, it is shown that a specific class of PSC patterns may reduce the PSO effectiveness to a level as lower as 36%. The analysis was conducted through a systematic approach involving the system simulation for different Environmental conditions. Besides that, to accurately represent the effects of the inherent stochasticity of the PSO, the simulation of each case was repeated 25 times considering different starting conditions. It is important to notice that, in general, these details are not properly exploited in most articles in the literature. Thus, the present analysis provides a deep insight on the role Environmental and stochastic effects on hybrid PSO-InC MPPT. For these analyses, it was considered a three-panel PV array driven by a boost converter and controlled by a hybrid PSO-InC MPPT. The hybrid PSO-InC is similar to the MPPT proposed in [20], though in our case it was not considered the dormant-mode approach. It is also presented in this article some dynamic results encompassing the transient behavior of the MMP for different conditions.

II. Circuit Description and Simulation Methodology

Fig. 1 presents a short description of the considered system in this paper. A boost converter drives three series-connected PV with the harvested energy stored into a battery bank. The PV-side capacitance C_{in} reduces the voltage ripple at the PV-array terminals, which has non-linear characteristics. Moreover, there are bypass diodes to avoid mismatches whenever one of the panels is shaded, and there is a blocking diode to prevent current inversion. Tables I and II present the parameters of the PV panels and the hardware settings. As for the MPPT, it is represented in Fig. 1 by the block GMPPT. Usually, GMPPT receives the measurements of the PV voltage and current, v_{pv} and i_{pv}, and returns the duty cycle, d. The simulations were carried out in the PowerSim simulator (PSIM), considering a sample time of 1 µs (1 MHz). In this condition, a 10 kHz carrier used to modulate the converter presents a maximum resolution of 0.001 in the duty cycle [22]. The measurements are obtained with a sampling rate of 50 kHz, yet the MPPT runs on a 50 Hz basis for the PSO part and 100 Hz for the InC. These differences are due to the 50-sample windowed averaging used for eliminating switching noises from v_{pv} and i_{pv}, which is better explained in the following section.

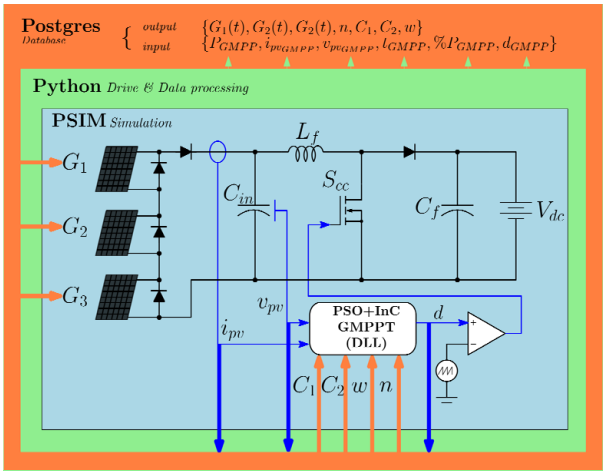

Figure 1. Architecture of simulation with three layers and proposed circuit

TABLE I. Panel Specifications

Parameter	Value
Number of cells	36
Maximum output power	140 W
Nominal voltage at MPP	17.7 V
Nominal current at MPP	7.91 A
Open circuit voltage (V_{OC})	22.1 V
Short-circuit current (I_{SC})	8.68 A
Thermal coefficient of V_{OC}	-0.36 %/C
Thermal coefficient of I_{SC}	0.6 %/C
Thermal coefficient of P_{MPP}	-0.46 %/C

TABLE II. Hardware Settings

Parameter	Symbol	Value
Battery Bank voltage	V_{dc}	96 V
PV-side capacitor	C_{in}	480 µF
Boost-conv. Inductance	L_f	98 µH
Boost-conv. Capacitance	C_f	30 µF
Switching frequency		10 kHz
Duty-cycle resolution		0.01

In Fig. 1 there are also references to Python, PostgreSQL, and a dynamic-link library (DLL). Nevertheless, one may note that these tools were considered only for automation and implementation of the simulations. More specifically, a Python script was developed for calling the PSIM simulation several times, each one considering a different Environmental condition. Due to the amount of obtained data in some tests, it was decided to store these results in the database. Consequently, neither Python nor PostgreSQL, interfere with the control algorithms. Finally, the DLL implements the GMPPT algorithms compiled in C language.

III. Proposed Global MPPT Approach

The proposed MPPT algorithm combines two well-established searching approaches, InC and the PSO [21-22]. Firstly, the PSO algorithm explores a wide domain to find the neighborhood of the GMPP. Then, the incremental conductance algorithm conducts a fine search and track small oscillations in the maximum power point due to Environmental changes. A detailed description of the proposed algorithm is presented in Fig. 2, with the global and the local search loops highlighted.

The global search loop comprises both the initialization procedure and a PSO algorithm, already analyzed in [15], that might look over the entire domain for the neighborhood of the GMPP. In this regard, d_i and u_i are the position and velocity of a certain particle i, both of each updated accordingly to:

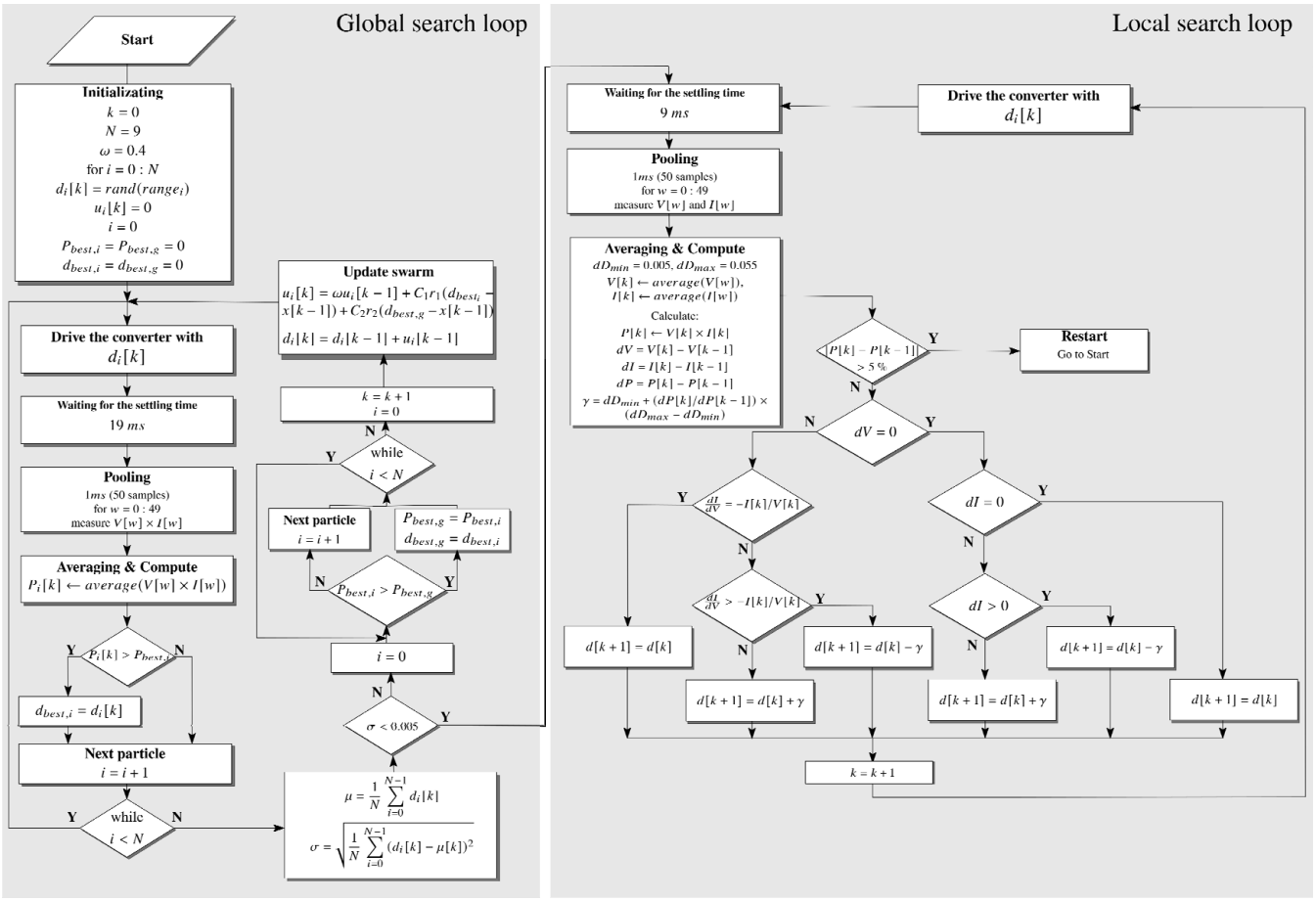

Figure 2. MPPT flowchart with the local and the global search for N particles. The global search represents the process of going from particle to particle testing the power response. The local search loop implements the InC algorithm to keep tracking small changes in the system

$$u_i = wu_i[k-1] + C_1 r_1 (d_{best,i} - x[k-1]) + C_2 r_2 (d_{best,g} - x[k-1]) \quad (1)$$

$$d_i[k] = d_i[k-1] + u_i[k] \quad (2)$$

Notice that u_i presents two components that depend on random variables (r_1 e r_2). The first, $C_1 r_1 (d_{best,i} - x[k-1])$, is the cognitive component and the second, $C_2 r_2 (d_{best,g} - x[k-1])$, is the social component. In this sense, C_1 and C_2 are constants that weigh the tendency of a particle to return to its individual best solution $(d_{best,i})$ or to follow towards the flock best solution $(d_{best,g})$. Also, in (1), ω is an inertial constant that weighs the tendency of a particle to remain with its previous velocity.

Note that the letter N in the flowchart indicates the total amount of particles and the letter k is the computational eon, that is, the corresponding iteration of the global search. Continuing, $d_i[k]$ is the particle i position in the iteration k, and the same rule of thumbs can be used to describe the other variables in the diagram. Of course, the position $d_i[k]$ corresponds to the duty-cycle associated to the particle, and $P_i[k]$ is the power produced in its turn at a given eon. To reduce the oscillation effects, transients, and switching-related noise alike, $P_i[k]$ is computed considering the windowed average approach after a preestablished delay, in this case, 19 ms. Each particle stores their best performance ($P_{best,i}$ and $d_{best,i}$) along the eons and the PSO-algorithm as a whole store the best performance ($P_{best,g}$ and $d_{best,g}$). These values are used in (1) to compute the velocity of the particles. For deciding when the global search should be switched off, it was applied the standard deviation approach. For this matter, the average position $\mu[k]$ of all the particles along with its standard deviation $\sigma[k]$ are computed at every eon, as shown in the flowchart. Then, it was established that the algorithm should swap to the local search when sigma becomes under 0.005, which in turn avoid the chattering-like pattern commonly observed in PSO-based MPPTs. The condition $\sigma < 0.005$ implies that all particles are in a small neighborhood around the GMPP. The hyper parameters of the PSO were adjusted [14] and listed in Table III.

TABLE III. PSO PARAMETERS

n	C_1	C_2	ω
9	1.6	1.6	0.4

The local search, on the other hand, is based on an InC algorithm for which the initial duty-cycle corresponds to the final value of $d_{best,g}$ computed during the global search. Its implementation is based on the following result:

$$\frac{dP}{dV} = \frac{d(Vi)}{dV} = i\frac{dV}{dV} + \frac{Vdi}{dV} = i + \frac{Vdi}{dV} \quad (3)$$

where, V, i, and P are basically the PV-array voltage, current, and power. Notice that dP/dV tends to zero when the system approaches the MPP. Besides that, di/dV is either positive or negative depending on whether the system is operating on the right or on the left side of the MPP respectively. Combining this information is possible to implement the algorithm which is represented in the local-search group of (3). More details on the InC MPPT can be found in [23], and [25].

IV. Simulation Results

This section presents several simulations to analyze the effectiveness aspects of the PSO-InC MPPT, including the details for each one of the operational conditions. For all the test cases, it was considered the introduced system in section II.

A. Evaluation of Stochastic and Environmental Effects

For this evaluation, we considered several simulations for a group of different scenarios. At first, it is necessary to explain that the term scenario used here indicates a different shading pattern. Thus, there were considered 120 scenarios grouped into eight classes, as presented in Table IV. The numbers 1, 2, and 3 in Table IV refer to the MPPs present in the P×V curve, with being MPP_1 the leftmost and MPP_3 the rightmost when the PSC imposes a three-MPP pattern.

Table IV. Patterns (Classes)

Two-MPP pattern		Three-MPP pattern					
12	**21**	**123**	**132**	**213**	**231**	**312**	**321**
$P_{MPP1} > P_{MPP2}$	$P_{MPP2} > P_{MPP1}$	$P_{MPP1} > P_{MPP2} > P_{MPP3}$	$P_{MPP1} > P_{MPP3} > P_{MPP2}$	$P_{MPP2} > P_{MPP1} > P_{MPP3}$	$P_{MPP2} > P_{MPP3} > P_{MPP1}$	$P_{MPP3} > P_{MPP1} > P_{MPP2}$	$P_{MPP3} > P_{MPP2} > P_{MPP1}$

Fig. 3 illustrates with examples each of the eight classes considered in the analysis. Notice that class 132 is characterized by presenting $P_{MPP1} > P_{MPP3} > P_{MPP2}$, and the analogous rule is also applied for the others.

Based on Table V, one may note five sub-classes, labeled as A-E. For each scenario, there is a power difference between the GMPP and the second highest MPP. These differences are within the margins of 5%, 5-10%, 10-15%, 15-20%, and over 20%. The objective was to spot characteristics of the problem that might compromise the effectiveness of the proposed MPPT. There is also a PSC-free scenario, not indicated in Fig. 3 nor in Table IV, used as a reference to the comparisons. The stochastic effects in the positions of the particles can lead to different paths to the solution or even, in the worst case, derail the convergence of the algorithm. Thus, the considered scenarios were simulated 25 times, each one considering a different seed for the random parts of the algorithm. This strategy sheds light on the capability of the proposed MPPT to find the GMPP following different paths.

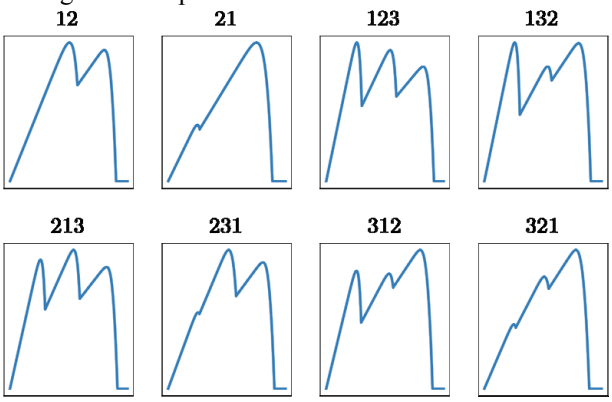

Figure 3. LMPP patterns in the P×V curve, considered for instance "12" meaning $P_{MPP1} > P_{MPP2}$

Table VI summarizes the number of cases in which the MPPT converged for the GMPP. The timeout of convergence corresponds to 10 s. The remaining cases were in the group that did not converge. Thus, the general result indicated 89% of efficacy, where the convergency was achieved in 2697 out of 3025 simulations. The results are even higher if only the subclasses C-E are considered. In these cases, the differences between the MPPs make the PSO task easier. The subclasses A and B, on the other hand, present more discreet results, scoring 70% and 80% of efficacy in finding the GMPP. Notice that the narrowing of the difference between the two highest peaks is responsible for the observed reduction in efficacy. This conclusion is aligned with the fact that, among the cases where the GMPP was not found, the second highest MPP was the dominant result. Consequently, it is possible to state that error in finding the GMPP caused less than 5% difference in the harvested power for cases in subclass A, and between 5% to 10% for the cases in the subclass B.

Classes 21 and 312 stand out due to the poor performance among the eight different classes. In the worst situation, which corresponds to class 312, the GMPP was achieved in 67% of the cases. It is important to notice that the MPPT performance for this class was worse than the others even in the easy-tracking cases, i.e., subclasses C-D. For comparison, the classes 312.B and 21.B presented, respectively, 80% and 85% rate of convergence to the GMPP when the entire subclass-B rate was 94%. The issue with the class 312 is due to a combination of the P×V curve inherent characteristic and the initial displacement of the particles. The MPP_3, the largest power peak in class 312, in general occupy a narrow neighborhood nearby the open circuit voltage. On the other hand, MPP_1, which corresponds to the second largest peak, dominates a wider fraction of the domain in a region diametrically opposed to the MPP_3. As the MPP_1 neighborhood is wider, it accommodates more particles in the initial eon than the MPP_3 counterpart.

Table V. LMPP Patterns (Sub-Classes)

Sub - class	MPP difference
A	<5 %
B	5-10 %
C	10-15 %
D	15-20 %
E	>20 %

Consequently, the probability of a particle nearby MPP_1 spot the best position in the initial eon is greater than the other way around. This factor can cause a bias in the PSO algorithm, generating a large acceleration that might force the particles nearby MPP_3 inward MPP_2, overlooking the GMPP. The MPP_2 is the smallest of all the peaks, thus, the particles around it are prone to be overshadowed by those around MPP_1 in the following eons, strengthen the march inward MPP_1. Of course, this phenomenon has a probabilistic nature and is prevalent when the difference between P_{MPP1} and P_{MPP3} are small (subclasses A and B), as can be seen in Table VI. It is important to reinforce the significant role of the distance between the regions of the two largest peaks in this issue. The initial bias might also be a fact in class 321, yet the small distance between the major peaks, MPP_3 and MPP_2, reduces the chances of larger

TABLE VI. CONVERGENCE TO THE GMPP

Class / Subclass	1	12	21	123	132	213	231	312	321	Total	% of Total
A- < 5 %		64	33	50	64	47	73	33	58	422	70 %
B- 5 %-10 %		75	51	74	73	71	75	27	71	517	86 %
C- 10 %-15 %		75	64	72	71	72	75	60	73	562	94 %
D- 15 %-20 %		75	75	75	75	73	75	64	74	586	98 %
E- > 20 %		75	68	74	75	75	75	68	75	585	98 %
STC	25									25	100 %
Total	25	364	291	345	358	338	373	252	351	2697	89 %
% of Total	100 %	97 %	78 %	92 %	95 %	90 %	99 %	67 %	94 %	89 %	

accelerations that could derail the PSO search. A potential solution for class 312 issue would be populate the region nearby MPP_3 with more particles. Nonetheless, this action would cause bias issues in other classes. Another possible solution would be increasing the weight of the inertial term in (1) in relation to the other terms, reducing the acceleration of the particles. This action makes the particles hover around their original regions for a long period of time, favoriting the particles around the GMPP. As a side effect, the convergence time would be increased for all the classes.

When analyzing the convergence time, it was verified an average value of 3.71 s, with a standard deviation of 0.968 s. In Fig. 4 and Fig. 5 one may see box plots indicating the results by classes and subclasses, respectively. The white circle within each box corresponds to the average convergence time for that class/sub-class. Note that the obtained results from classes 21 and 312 were worsen than the others. In both cases, the average convergence time surpassed 4 s, and the standard deviation reached 1.18 s and 1.51 s, respectively. Furthermore, note the difference between the mean time and median time (indicated by the central line in each box). For class 312, for instance, the median time was about 1s lower than the class average. Moreover, in half of the cases, the convergence was achieved in 3.7 s, approximately. On the other hand, class 12 presented the best results, with an average convergence time lower than 3.5 s. As for the subclasses, according to Fig. 5, class A was more time-consuming, requiring, in general, 0.5 s more than the other classes to converge.

B. Time-Response Analysis

This section contains some of the time-domain results obtained to verify the dynamic behavior of the GMPP tracking. In this case, it was considered a static PSC where the equivalent irradiance at each panel is equal to G_1 = 100 W/m^2, G_2 = 300 W/m^2, and G_3 = 700 W/m^2. The theoretical maximum power for this case is $GMPP_{th1}$ = 98.82 W, which was obtained with the PV-array voltage v_{gmpp_th} = 17.39 V, as shown in Fig. 6. Considering the effectiveness of the algorithm, the MPPT was able to harvest 99.92 % of the available energy, such that, with the global MPPT achieved, the PV system produces 98.75 W, as indicated in Fig. 7. From the time instant in which the PSO converged, the global MPPT is disabled and replaced by a local MPPT.

Fig. 7 presents the time response for this test case, for which it is observed the typical chattering characteristic of the PSO throughout the period that goes from 0.25 s, when the MPPT was enabled, to 1.845 s, when the PSO converged. This chattering represents the effect of the converter trying the values of the duty cycle associated with different particles. As the particles converge to the neighborhood of the GMPP, the converter starts being driven by a smooth duty cycle, and the chattering dyes out. As already mentioned, the local MPPT was enabled at t=1.845 s, though its role, in this case, is negligible once the PSO virtually achieved the GMPP (99.92% of the theoretical GMPP). Notice that the local MPPT is expected to play an important role when there are gradual changes in the Environmental conditions.

One may note the acquired power presenting a high-frequency oscillation (ripple) of different amplitudes in some cycle periods. It compromises the acquired samples of the PV-power applied for determining its average component. Fig. 8 depicts this effect in a zoomed vision.

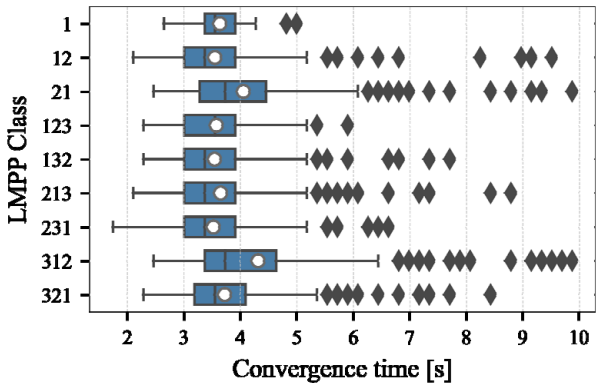

Figure 4. Convergence time by class. Mean value plotted as the white circle

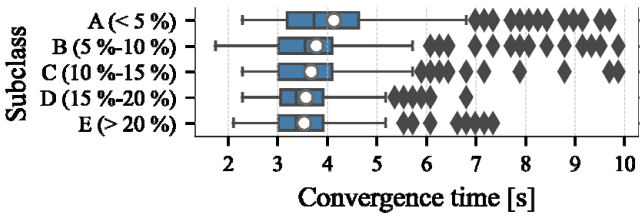

Figure 5. Convergence time by subclass. Mean value plotted as the white circle

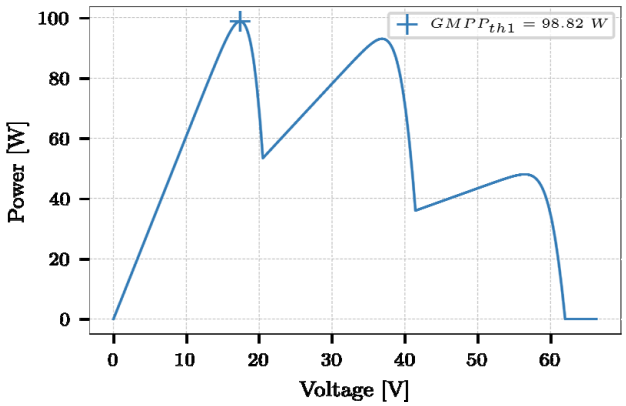

Figure 6. Power-Voltage characteristic of one of power pattern "123" with panels irradiated with constant values of G_1 = 100W/m2, G_2 = 300W/m2 and G_3 = 700W/m2. Theoretical $GMPP_{th1}$ = 98.82W

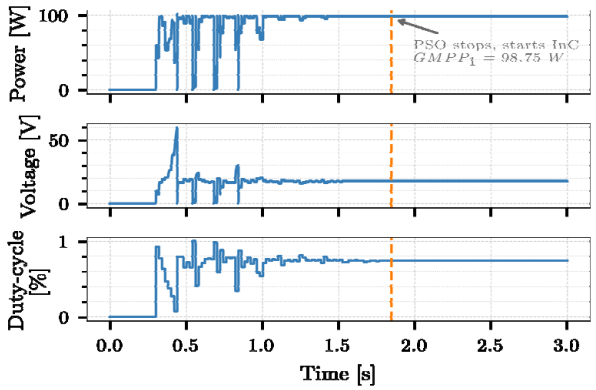

Figure 7. Output power and duty cycle of case static PSC. Track 99.92 % of $GMPP_{th}$

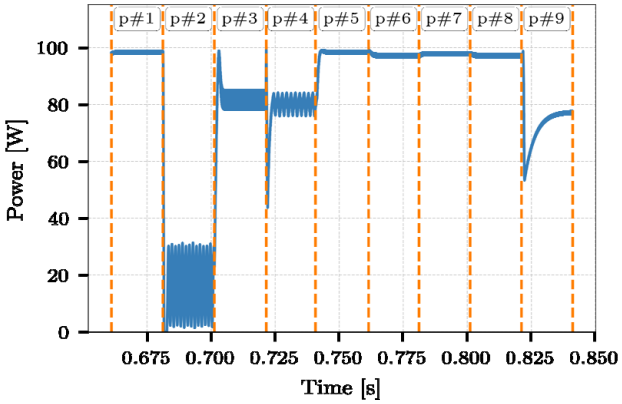

Figure 8. Zoomed view of the acquired power, with the chattering effect highlighted due to the PWM switching resulting in oscillating components. "p #n" indicates the particle number

C. Dynamic Response of the MPPT for an Abrupt Change in the Irradiance

In this test case, occurs 50% reduction in the global irradiance intensity at t = 5 s. Initially, the panels are radiated with G_1 = 200 W/m^2, G_2 = 300 W/m^2, and G_3 = 800 W/m^2, leading to a power profile with default "132" and a maximum theoretical power $GMPP_{th1}$ equal to 112.73 W. Thus, with 50 % reduction in the global irradiance, the new irradiance profile becomes G_1 = 100 W/m^2, G_2 = 150 W/m^2 and G_3 = 400 W/m^2 and the maximum available power drops to $GMPP_{th2}$ = 56.36 W, as illustrated in the P×V curve in Fig. 9.

The purpose of this test case is to reset the PSO-algorithm, without changing the pattern. As illustrated in Fig. 10, before the 50% of irradiance reduction, the maximum power corresponds to $GMPP_1$. In sequence, when this transient occurs, the PSO correctly identifies the new maximum power, $GMPP_2$, after 1.45 s.

D. Dynamic Response of the MPPT for an Abrupt Change in the Shading Pattern

For analyzing the process of reinitialization, the following test case was conducted. Initially, the panels were irradiated with G_1 = 600 W/m^2, G_2 = 800 W/m^2, and G_3 = 1000 W/m^2, leading to a power profile in class "321". At t = 5 s, the irradiances decreased so that G_1 = 200 W/m², G_2 = 300 W/m² e G_3 = 800 W/m², which is a pattern that belongs to the class "132". Fig. 11 depicts the P×V curves related to these patterns. Fig. 12 shows that the convergence process for the first shading pattern is about 1.70 s long.

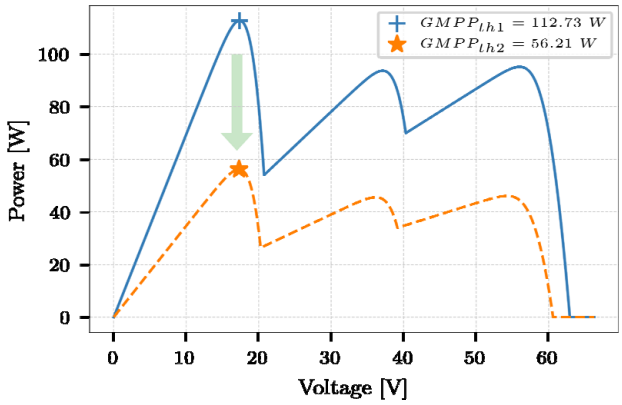

Figure 9. Irradiance pattern showing first and second profiles, both with "132" shape

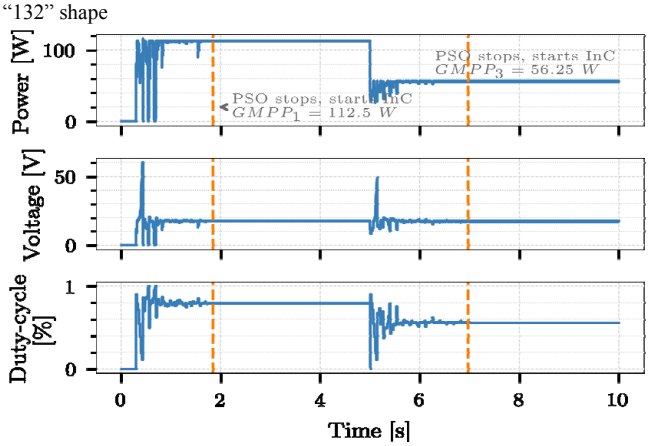

Figure 10. Time response of abrupt change in irradiance levels with same pattern. Tracked 99.98 %$GMPP_{th1}$ and 100 %$GMPP_{th2}$

For better illustration, the global MPP for this pattern is named GMPP$_1$ in the figure, whereas $GMPP_2$ is used for the global MPP of the second pattern. In this case, the MPPT leads the system to produce 282.25 W, corresponding to 100 % of the maximum theoretical power for this profile. At t = 5 s, there was a change in the shading pattern. This modification triggered the PSO algorithm to identify the new global maximum. Fig. 12 shows the MPPT producing the correct maximum power ($GMPP_2$) after a 1.41 s period. In this condition, the produced power corresponds to 112.5 W or 99.79 % of the theoretical MPP.

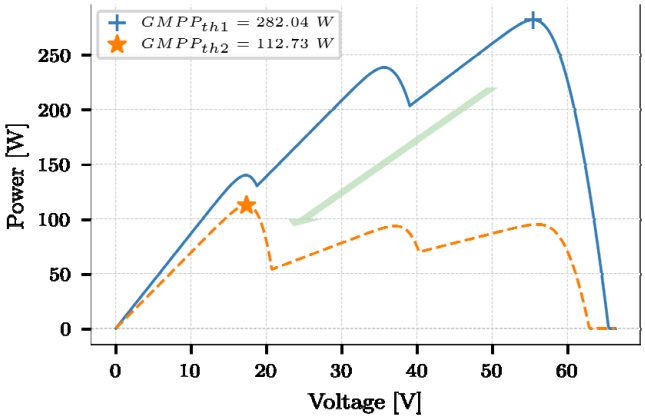

Figure 11. Power profiles used: in blue line first power profile of "321" and in dashed orange second power profile with "132" shape

E. Dynamic Response of the MPPT for a Gradual Change in the Irradiance

In this test case, the irradiance pattern corresponds to the

one illustrated in the upper chart of Fig. 13. One may note the irradiances follow an up-rising behavior for 0 < t < 5 s.

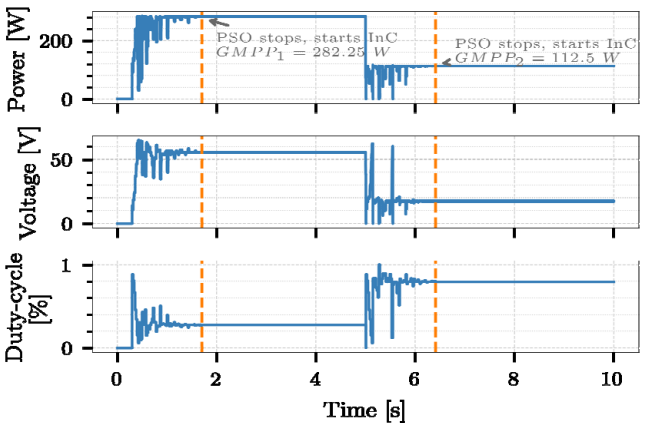

Figure 12. Convergency process when an abrupt change occurs in the shade pattern. Tracked 100 %$GMPP_{th1}$ and 99.79 %$GMPP_{th2}$

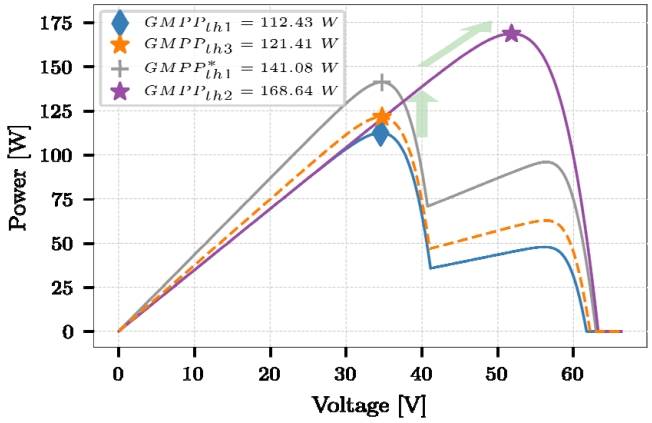

Figure 13. Irradiance pattern showing the start and end mark values of $GMPP_{th1}$ and $GMPP_{th2}$. In t = 5 s the pattern without shade ($GMPP_{th3}$) is used

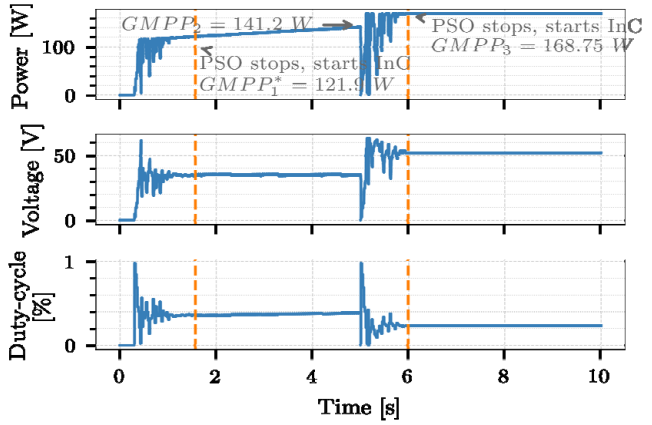

Figure 14. Convergency process showing the transition between algorithms. At t = 1.7 s and t = 6.97 s the PSO stops and the InC takes place

The objective is to observe the functioning of the InC algorithm by adjusting the local maximum after identifying the global maximum through a smooth change in irradiance.

In the interval 0 < t < 5 s the irradiance is smoothly increased from 0 to 200 W/m^2, starting from G_1 = 100 W/m^2, G_2 = 400 W/m^2 and G_3 = 400 W/m^2 at t = 0 s ($GMPP_{th1}$ = 112.43 W) to G_1 = 200 W/m^2, G_2 = 500 W/m^2 and G_3 = 500 W/m^2 at t = 5 s ($GMPP_{th2}$ = 141.08 W). At this same instant, a disturbance replaces the partial shading with G_1 = 400 W/m^2, G_2 = 400 W/m^2 and G_3 = 400 W/m^2 ($GMPP_{th3}$ = 168.64 W). In sequence, Fig. 14 depicts the P×V curves in the time domain.

V. CONCLUSION

This article addressed an analysis of the hybrid PSO-InC MPPT when the system is under different patterns of PSC. Once the PSO partially relies on the random behaviour to find the global MPP, each PSC pattern was simulated 25 times, each one considering a different starting condition, i.e., different values of seed for the random variables.

The results show that the MPPT presents a rate of effectiveness of nearly 89%, in other words, the algorithm finds the GMPP in 89% of the cases. Nonetheless, it was spotted a particular scenario in which the rate drops to 67%. In this scenario, the PV system presents a partial shading condition that creates three MPPs, where the rightmost in the P×V curve is the highest, the central MPP is the lowest, and the leftmost presents the intermediary amplitude (class 312).

As for the convergence time of the algorithm, the average, including all the simulated cases, was 3.71 s with a standard deviation equal to 0.968 s. When analyzing only the results within class 312, the convergence time surpassed 4 s and the standard deviation neared 1.5 s. Among the subclasses, A was the one with a higher average convergence time, consuming roughly half a second more than the other subclasses. It is important to notice that the difference between the two highest peaks in the P×V curves of subclass A is under 5 %. Consequently, the PSO searching tends to be slower.

The paper also presented simulation results showing the performance of the hybrid PSO-InC MPPT when the system undergoes abrupt and gradual changes in the radiance level, besides abrupt changes in the partial-shading pattern. The major outcome of this analysis is showing the role of the InC algorithm in the hybrid MPPT: it tracks the MPP when a small change in the radiance level occurs, avoiding in these cases an unnecessary time-consuming cycle of PSO.

REFERENCES

[1] A. Jäger-Waldau, "Snapshot of photovoltaics-March 2017," no. 5, p. 9, 2017. doi:10.3390/su9050783

[2] S. Jiang, C. Wan, C. Chen, E. Cao, and Y. Song, "Distributed photovoltaic generation in the electricity market: status, mode and strategy," CSEE JPES, vol. 4, no. 3, pp. 263–272, Sep. 2018. doi:10.17775/CSEEJPES.2018.00600

[3] R. B. Bollipo, S. Mikkili, and P. K. Bonthagorla, "Critical review on PV MPPT techniques: classical, intelligent and optimisation," IET Renewable Power Generation, vol. 14, no. 9, pp. 1433–1452, Jul. 2020. doi:10.1049/iet-rpg.2019.1163

[4] R. Panigrahi, S. K. Mishra, S. C. Srivastava, A. K. Srivastava, and N. N. Schulz, "Grid integration of small-scale photovoltaic systems in secondary distribution network—a review," IEEE Trans. on Ind. Applicat., vol. 56, no. 3, pp. 3178–3195, May 2020. doi:10.1109/TIA.2020.2979789

[5] P. Nammalvar and S. Ramkumar, "Parameter improved particle swarm optimization based direct-current vector control strategy for solar PV system," AECE, vol. 18, no. 1, pp. 105–112, 2018. doi:10.4316/AECE.2018.01013

[6] J. Teo, R. Tan, V. Mok, V. Ramachandaramurthy, and C. Tan, "Impact of partial shading on the P-V characteristics and the maximum power of a photovoltaic string," Energies, vol. 11, no. 7, p. 1860, Jul. 2018. doi:10.3390/en11071860

[7] S. R. Pendem and S. Mikkili, "Modelling and performance assessment of PV array topologies under partial shading conditions to mitigate the mismatching power losses," Solar Energy, vol. 160, pp. 303–321, Jan. 2018. doi:org/10.1016/j.solener.2017.12.010

[8] H. Patel and V. Agarwal, "Maximum Power Point Tracking Scheme for PV Systems Operating Under Partially Shaded Conditions," IEEE Trans. Ind. Electron, vol. 55, no. 4, pp. 1689–1698, Apr. 2008. doi:10.1109/TIE.2008.917118

[9] K. Chen, S. Tian, Y. Cheng, and L. Bai, "An improved MPPT controller for photovoltaic system under partial shading condition," IEEE Trans. Sustain. Energy, vol. 5, no. 3, pp. 978–985, Jul. 2014. doi:10.1109/TSTE.2014.2315653

[10] H. Li, D. Yang, W. Su, J. Lu, and X. Yu, "An overall distribution particle swarm optimization MPPT algorithm for photovoltaic system under partial shading," IEEE Trans. Ind. Electron., vol. 66, no. 1, pp. 265–275, Jan. 2019. doi:10.1109/TIE.2018.2829668

[11] A. Khare and S. Rangnekar, "A review of particle swarm optimization and its applications in solar photovoltaic system," Applied Soft Computing, vol. 13, no. 5, pp. 2997–3006, May 2013. doi:10.1016/j.asoc.2012.11.033

[12] V. N. Lal and S. N. Singh, "Modified particle swarm optimisation□based maximum power point tracking controller for single□stage utility□scale photovoltaic system with reactive power injection capability," IET Renewable Power Generation, vol. 10, no. 7, pp. 899–907, Aug. 2016. doi:10.1049/iet-rpg.2015.0346

[13] A. Mohapatra, B. Nayak, P. Das, and K. B. Mohanty, "A review on MPPT techniques of PV system under partial shading condition," Renewable and Sustainable Energy Reviews, vol. 80, pp. 854–867, Dec. 2017. doi:10.1016/j.rser.2017.05.083

[14] A. L. M. Leopoldino, C. Magalhães Freitas, and L. F. Corrêa Monteiro, "On the effects of parameter adjustment on the performance of PSO-based MPPT of a PV-energy generation system," in Green Energy and Networking, vol. 269, J. L. Afonso, V. Monteiro, and J. G. Pinto, Eds. Cham: Springer International Publishing, 2019, pp. 175–192. doi:10.1007/978-3-030-12950-7_14

[15] A. L. M. Leopoldino, C. Magalhães Freitas, and L. F. Corrêa Monteiro, "On the effects of hyper-parameters adjustments to the PSO-GMPPT algorithm for a photovoltaic system under partial shading conditions," EAI Endorsed Trans. Energy Web, vol. 7, no. 25, p. 160981, Jan. 2020. doi:10.4108/eai.13-7-2018.160981

[16] K. Sundareswaran, V. Vignesh Kumar, and S. Palani, "Application of a combined particle swarm optimization and Perturb and Observe method for MPPT in PV systems under partial shading conditions," Renewable Energy, vol. 75, pp. 308–317, Mar. 2015. doi:10.1016/j.renene.2014.09.044

[17] K. L. Lian, J. H. Jhang, and I. S. Tian, "A maximum power point tracking method based on Perturb-and-Observe combined with particle swarm optimization," IEEE J. Photovoltaics, vol. 4, no. 2, pp. 626–633, Mar. 2014. doi:10.1109/JPHOTOV.2013.2297513

[18] S. Z. Mirbagheri, M. Aldeen, and S. Saha, "A PSO-based MPPT re-initialised by incremental conductance method for a standalone PV system," in 2015 23rd Mediterranean Conference on Control and Automation (MED), Torremolinos, Malaga, Spain, Jun. 2015, pp. 298–303. doi:10.1109/MED.2015.7158766

[19] M. Abdulkadir and A. H. M. Yatim, "Hybrid maximum power point tracking technique based on PSO and incremental conductance," in 2014 IEEE Conference on Energy Conversion (CENCON), Johor Bahru, Malaysia, Oct. 2014, pp. 271–276. doi:10.1109/CENCON.2014.6967514

[20] C. Manickam, G. R. Raman, G. P. Raman, S. I. Ganesan, and C. Nagamani, "A hybrid algorithm for tracking of GMPP based on P&O and PSO with reduced power oscillation in string inverters," IEEE Trans. Ind. Electron., vol. 63, no. 10, pp. 6097–6106, Oct. 2016. doi:10.1109/TIE.2016.2590382

[21] J. Shi, W. Zhang, Y. Zhang, F. Xue, and T. Yang, "MPPT for PV systems based on a dormant PSO algorithm," Electric Power Systems Research, vol. 123, pp. 100–107, Jun. 2015. doi:10.1016/j.epsr.2015.02.001

[22] S. Buso and P. Mattavelli, "Digital control in power electronics," Synthesis Lectures on Power Electronics, vol. 1, no. 1, pp. 1–158, Jan. 2006. doi:10.2200/S00047ED1V01Y200609PEL002

[23] F. Liu, S. Duan, F. Liu, B. Liu, and Y. Kang, "A variable step size INC MPPT method for PV systems," IEEE Trans. Ind. Electron., vol. 55, no. 7, pp. 2622–2628, Jul. 2008. doi:10.1109/TIE.2008.920550

[24] A. L. M. Leopoldino, "Estratégia híbrida para rastreamento de máxima potência em sistemas fotovoltaicos sombreados," Universidade do Estado do Rio de Janeiro, Feb. 27, 2019. Accessed: Apr. 07, 2021. [Online]. Available: http://www.bdtd.uerj.br/handle/1/11761

[25] L. F. C. Monteiro, C. M. Freitas, and M. D. Bellar, "Improvements on the incremental conductance MPPT method applied to a PV string with single-phase to three-phase converter for rural grid applications," Advances in Electrical and Computer Engineering, vol. 19, no. 1, p. 8, 2019. doi:10.4316/AECE.2019.01009